Systemic dissemination, reproductive tissue tropism, and gestational stage-dependent placental responses during Mayaro virus infection in a murine model

Arévalo A.P.[1], Perbolianachis P.[2,3], Pórfido J.L.[1], Pereira-Gómez M.[2,4], Greif G.[5], Hurtado J.[2,3], Fajardo A.[2,3], Varela B.[6], Verdes J.M.[6], Moratorio G.[2,3*], Crispo M[1*].

[1]Laboratory Animal Biotechnology Unit, Institut Pasteur de Montevideo, Uruguay

[2]Experimental Virus Evolution Laboratory, Institut Pasteur de Montevideo, Uruguay

[3]Laboratory of Molecular Virology, Nuclear Research Center, Faculty of Sciences, Udelar

[4]Microbiology Unit, Department of Pathobiology, Faculty of Veterinary Medicine, Udelar

[5]Host-Pathogen Interaction Laboratory, Institut Pasteur de Montevideo, Uruguay

[6]Pathology Unit, Department of Pathobiology, Faculty of Veterinary Medicine, Udelar

[*] Corresponding authors: crispo@pasteur.edu.uy; moratorio@pasteur.edu.uy

ABSTRACT

Mayaro virus (MAYV) is an emerging mosquito-borne alphavirus associated with acute febrile illness and persistent arthralgia, with increasing reports in Latin America and potential for geographic expansion. However, its dissemination dynamics, tissue tropism, and transmission routes remain incompletely defined. Here, we developed a murine model to characterize systemic viral dissemination, tissue tropism, and the impact of gestational stage on maternal–fetal infection. A nanoluciferase-expressing MAYV reporter enabled non-invasive *in vivo* imaging, revealing rapid and widespread systemic dissemination under controlled conditions. Complementary infection with wild-type (WT) virus confirmed broad tropism across lymphoid, musculoskeletal, and reproductive tissues. At 24 hours post-infection (hpi), viral distribution was relatively homogeneous, whereas at 48 hpi, tissue-specific accumulation was evident, including increased viral loads in male reproductive tissues. Hematological and biochemical analyses indicated early systemic alterations consistent with inflammatory and immune cell redistribution. Infectious viral particles were detected in reproductive tissues of both sexes, supporting the plausibility of non-vector transmission. Gestational stage significantly influenced infection outcomes: early gestation (infected at 7.5–8.5 dpc; analyzed at 9.5–10.5 dpc) was associated with placental permissiveness and detection of infective virus in fetal tissues, whereas mid-gestation (infected at 13.5–14.5 dpc; analyzed at 15.5–16.5 dpc) showed no detectable infectious virus in fetuses despite sustained viral presence in maternal and placental compartments. Together, these findings establish a robust experimental framework for investigating MAYV pathogenesis and identify tissue tropism, sex-related differences, and gestational stage as key determinants of viral dissemination and maternal–fetal infection.

KEYWORDS: Mayaro virus; viral pathogenesis; Emerging arbovirus; Vertical transmission; Systemic dissemination; Placental infection; Murine model; *in vivo* imaging

AUTHOR SUMMARY

Mayaro virus is an emerging mosquito-borne virus that causes fever and long-lasting joint pain, with increasing reports in Latin America and potential for wider geographic spread. Despite its growing importance, several key aspects of MAYV pathogenesis remain to be fully elucidated, including the mechanisms driving systemic dissemination and tissue tropism, as well as its potential to impact pregnancy or be transmitted through non-vector routes. We used a mouse model with a luminescent reporter virus to track Mayaro virus dissemination in vivo, revealing rapid and widespread spread across multiple tissues. In studies using wild-type virus, detection occurred not only in muscle and immune-related organs but also in reproductive tissues of both males and females. Over time, viral distribution shifted from an initially uniform pattern to a more tissue-specific accumulation, including increased viral load in reproductive tissues. Importantly, gestational stage influenced viral distribution. When infection occurred early in gestation, infectious viral particles were detected in fetal tissues. In contrast, at later stages of pregnancy, infectious virus was no longer detectable in fetuses, even though it remained present in maternal and placental tissues. Altogether, these findings improve our understanding of Mayaro virus infection and highlight gestational timing as a key factor determining the risk of fetal exposure. They also support the potential for alternative transmission routes and provide a framework for future studies on this emerging virus.

INTRODUCTION

Mayaro virus (MAYV), an emerging arbovirus of the *Alphavirus* genus and *Togaviridae* family, was first identified in Trinidad and Tobago in 1954 and has since been responsible for sporadic outbreaks across Central and South America. Imported cases have also been reported in Europe and North America, raising concerns at the international public health level as reflected in the epidemiological alert issued by the Pan American Health Organization / World Health Organization in May 2019, which emphasized the need to strengthen epidemiological surveillance and laboratory diagnostic capacity (1). The virus has already been detected in Brazil, Peru, Venezuela, Suriname, Colombia, Ecuador, Bolivia, and Panama, with serological evidence also reported in Costa Rica, Guatemala, Mexico, and Haiti (2–5). Multiple anthropogenic factors—including climate change, urbanization, human mobility, and the expanding distribution of mosquito vectors such as *Aedes aegypti* and *Aedes albopictus*—contribute to the increasing risk of MAYV geographic expansion, even in countries without active transmission, such as Uruguay (6,7). A recent study estimated that 58.9 million people in Latin America reside in ecologically suitable areas for MAYV transmission (6–8). From a genomic perspective, MAYV possesses a positive-sense single-stranded RNA genome of approximately 11.5 kb, which encodes both non-structural (nsP1–nsP4) and structural proteins (CP, E3, E2, TF, 6k, and E1) through two open reading frames (ORFs). The virion is enveloped in a lipid membrane containing E1 and E2 glycoproteins and exhibits high genetic plasticity, which facilitates its adaptation to a broad range of hosts. The viral replication cycle begins with the fusion of the viral envelope to the host cell membrane, followed by translation of viral proteins and the assembly of new virions. MAYV is classified into three genotypes: D (dispersed), L (limited), and N (new), the latter identified in Peru (9–14). In addition to its sylvatic cycle, MAYV is proposed to establish urban transmission

through vectors such as *Aedes spp.*, *Culex spp.*, and *Sabethes spp.*, with potential vertebrate reservoirs including marsupials, rodents, birds and alligators (15–17).

Clinically, Mayaro disease is generally a self-limiting illness characterized by fever, rash, headache, photophobia, myalgia and persistent polyarthralgia, which may last for months or even years, significantly impacting patients' quality of life. Hemorrhagic and neurological complications, as well as myocarditis, have also been reported (18). The clinical similarity to other arboviral diseases, such as Dengue and Chikungunya, combined with limited diagnostic capacity in endemic regions, hinders accurate differential diagnosis and contributes to underestimation of the actual disease burden (18,19). Beyond its typical acute presentation, increasing evidence from other arboviral infections, including Zika and Chikungunya viruses (ZIKV; CHIKV), indicates that clinical outcomes and transmission dynamics may extend beyond the classical vector-borne paradigm, raising questions about the potential involvement of vulnerable populations such as pregnant women and neonates (20–23). Although no specific antiviral treatments or licensed vaccines are currently available, several vaccine candidates are under development, with sustained epidemiological surveillance remaining essential to anticipate and mitigate future outbreaks (3,9,24).

Animal models, particularly murine species, have been instrumental in elucidating the pathogenesis of MAYV and in the preclinical evaluation of therapeutic and vaccine candidates. These models faithfully reproduce hallmark clinical manifestations—including ruffled fur, altered gait, and ocular irritation—as well as key histopathological features such as arthritis, myositis and tenosynovitis (25,26). Disease outcomes vary depending on host age and immune status (25,27–29). While the musculoskeletal system represents the site of the most evident clinical damage, the liver and spleen act as major systemic sites of viral replication, functioning as central hubs for Mayaro virus

117 amplification and dissemination (10,15,28,30). The development of experimental
118 platforms that enable robust and reproducible antiviral testing is essential for advancing
119 MAYV research. In this context, the integration of *in vivo* imaging technologies
120 constitutes a major methodological advance, as it allows real-time, non-invasive
121 monitoring of viral dissemination dynamics using tagged viruses (27,31) .

122 Here, we establish and refine a murine model as a preclinical platform for the future
123 evaluation of antiviral drugs and therapeutic interventions against MAYV. To validate
124 early systemic dissemination under controlled conditions, we employed a nanoluciferase-
125 expressing MAYV reporter for longitudinal *in vivo* imaging. Complementary
126 experiments using wild-type MAYV were performed to characterize tissue tropism, viral
127 load, hematological and biochemical alterations, and placental transcriptional responses
128 following controlled infection. We further assessed gestational stage–dependent placental
129 permissiveness and explored the biological plausibility of vertical and sexual
130 transmission. We hypothesize that gestational timing modulates placental susceptibility
131 to MAYV, defining critical windows of maternal–fetal vulnerability. Together, this
132 integrated framework enables mechanistic investigation of systemic dissemination,
133 reproductive involvement, and maternal–fetal risk during MAYV infection.

134

135 MATERIALS AND METHODS

136 Ethics statement

137 All procedures and experiments were conducted in accordance with the Ethics Committee
138 on Animal Use of the Institut Pasteur de Montevideo (CEUAIP #010-22, in compliance

139 with National Law 18.611 "Procedures for the Use of Animals in Experimentation,
140 Teaching, and Scientific Research Activities" and strictly followed ARRIVE guidelines.

141 **MAYV infective clones**

142 This study employed wild-type MAYV and nano Luc-expressing MAYV (MAYV-nLuc)
143 infectious clones based on the TRVL 4675 strain, a genotype D virus originally isolated
144 from a human case in Trinidad in the 1950s and kindly provided by Dr. James Weger-
145 Lucarelli (31–33).

146 **Cell culture**

147 Vero cells were maintained in Dulbecco's Modified Eagle Medium (DMEM)
148 supplemented with 10% fetal bovine serum (FBS), penicillin (100 U/mL), and
149 streptomycin (100 µg/mL) and maintained at 37 °C, with 5% CO_2.

150 **Virus generation**

151 Infectious virus was rescued from both WT and MAYV-nLuc infectious clones by
152 transfection of Vero cells using Lipofectamine™ 3000 (Invitrogen), according to the
153 manufacturer's instructions. Viral supernatants were collected when transfected cells
154 exhibited ≈80% cytopathic effect (CPE) and stored at -80°C as passage P0.

155 Working viral stocks were generated by sequential infection of Vero cells to produce P1
156 and P2 passages. The P2 viral stocks were titrated by plaque assay, verified by sequencing
157 and stored at -80°C until further use.

158 **Mice**

159 BALB/cJ mice (#000651) were bred and maintained at the Laboratory Animal
160 Biotechnology Unit's animal facility of Institut Pasteur de Montevideo. Mice were housed
161 in IVC Isolator Biocontainment unit (ISOCAGE-N, Tecniplast, Milan, Italy) and

162 acclimatized for one week prior to the experimental procedures. The cages were prepared
163 with wood chip bedding (Toplit 6, SAFE, France), plastic tunnels as enrichment and paper
164 napkins as nesting material. Environmental conditions were maintained at 20 ± 1°C, with
165 30–70% relative humidity, and a 14/10-hour light/dark cycle. The mice were provided
166 with *ad libitum* autoclaved standard diet (D113, SAFE) and filtered, autoclaved water.
167 Mice were specific pathogen-free (SPF) certified by IDEXX (USA) quarterly, in
168 accordance with FELASA standards.

169 **Animal experimental design**

170 Intraperitoneal (i.p.) inoculation was selected to enable controlled and synchronized
171 assessment of early systemic dissemination of Mayaro virus under standardized
172 experimental conditions. Although this route does not reflect natural mosquito-borne
173 transmission, it enables precise dose administration and reproducible systemic exposure,
174 thereby facilitating analysis of early viral dissemination dynamics. A nanoluciferase-
175 expressing MAYV reporter (MAYV-nLuc) was employed for non-invasive *in vivo*
176 imaging. This reporter-based approach was used specifically to define spatial and
177 temporal dissemination patterns. Complementary experiments using wild-type MAYV
178 were subsequently performed to quantify infectious viral loads, characterize
179 hematological and biochemical alterations, and assess placental transcriptional responses
180 following controlled infection. Viral doses were optimized according to the specific
181 objectives of reporter-based imaging and pathogenesis studies. Sex-specific analyses
182 were incorporated where biologically relevant, including assessment of reproductive
183 tissue tropism and transmission experiments. This integrated experimental framework
184 enabled systematic evaluation of viral dissemination, reproductive involvement, and
185 gestational stage–dependent placental permissiveness (Fig 1).

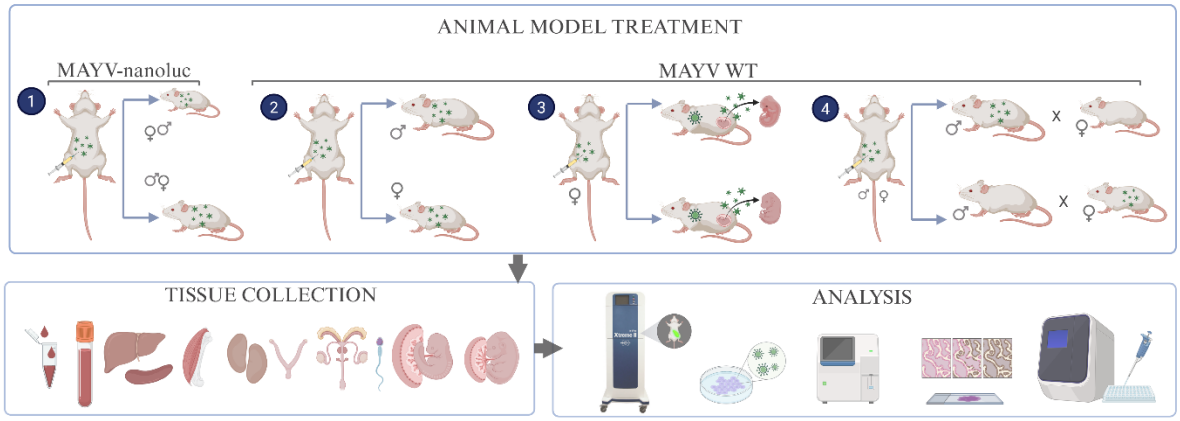

Figure 1. Experimental design for longitudinal assessment of early systemic dissemination of Mayaro virus in mice. Mice were i.p. inoculated with a bioluminescent Mayaro virus to enable longitudinal, non-invasive monitoring of early viral dissemination by *in vivo* imaging. Parallel groups were infected with wild-type Mayaro virus to evaluate tissue tropism and transmission-related outcomes. Blood and lymphoid, visceral, musculoskeletal, and reproductive tissues were collected for downstream analysis.

- ***In vivo* imaging evaluation with MAYV-nLuc infection**

In vivo bioluminescence imaging frequency was performed over a 10-day observation window to capture the peak of viral replication and the onset of immune responses associated with recovery from acute infection, based on previous reports (25,26,30). Age groups were selected according to their susceptibility to MAYV infection, with younger animals exhibiting higher susceptibility (34). For this study, four- and eight-week-old BALB/cJ female mice were i.p. infected with 1 x 10^4 PFU of MAYV-nLuc resuspended in 100 µL PBS (n=4 per age group). Mock-infected animals received PBS only (n = 2; one animal per age group). The viral dose was selected based on pilot optimization experiments to ensure robust reporter detection while maintaining animal welfare. To perform *in vivo* luminescence imaging, the animals were i.p. injected with 20 µg of Furimazine (TargetMol®, MA, USA) in 100 µL of PBS, anesthetized with isoflurane (3–4% for induction and 1-2 % for maintenance) and imaged at defined time points using an In-Vivo Xtreme II™ system (Bruker Daltonik GmbH, Billerica, MA, USA). Image

206 acquisition and analyses were performed using MolecularImaging software
207 V.7.5.3.22464 (Bruker Daltonik Gmbh, Billerica, MA, USA). Thresholds and exposure
208 times were kept constant across time points for longitudinal comparability.
209 Bioluminescent signal reflects reporter expression and may not directly correlate with
210 infectious viral titers. Imaging was performed at 1-, 2-, 6- and 10- day post infection (dpi).
211 Animals were necropsied at 6 dpi (n=2 per age group) and at 10 dpi (remaining animals).
212 Organs collected for confirmation of infectious viral particles included the liver, kidneys,
213 spleen, and *quadriceps femoris* muscle. Peripheral tissues exhibiting luminescent
214 signal—tail, ear, forelimb or hindlimb—were also sampled.

215 - **Viral tropism of Mayaro WT and health status**

216 Twelve BALB/cJ female and twelve BALB/cJ male mice (4 weeks old) were i.p. infected
217 with 1 x 10^5 PFU of MAYV WT resuspended in 100 µL of PBS (n=24). Mock-infected
218 mice received the PBS diluent alone (n=4). The viral dose was selected based on prior
219 pilot experiments as the lowest dose that consistently allowed detection of infectious viral
220 particles across tissues during acute infection. Blood samples were collected pre and post-
221 infection for hematological and biochemical parameter analyses at 0-, 24- and 48-hour
222 post infection (hpi). At 24 hpi, six animals of each sex were euthanized under deep
223 anesthesia induced by ketamine-xylazine mixture administered via the i.p. route
224 (ketamine 110 mg/kg; Pharmaservice, Ripoll Vet, Montevideo, Uruguay; xylazine 13
225 mg/kg; Seton 2%; Calier, Montevideo, Uruguay), followed by cervical dislocation.
226 Organs collected for quantification of infectious viral particles included the liver, kidneys,
227 spleen, *quadriceps femoris* muscle, ovaries, uterus, seminal vesicles and testes. The same
228 procedures were performed on the remaining animals at 48 hpi.

229 - **MAYV WT vertical transmission**

230 Seventeen BALB/cJ female mice (8-weeks old) were synchronized in their estrous cycle
231 by exposing them to male dirty bedding for 72 h prior to mating (35). Mating was then
232 performed by placing one proven male in a cage with two females for 48 h, and the
233 presence of a vaginal plug was checked daily from the following morning as a positive
234 sign of mating to be considered day 0.5 of pregnancy. At 7.5-8.5-day post-coitum (dpc),
235 six females were i.p. infected with 1 x 10^5 PFU of MAYV WT resuspended in 100 µL of
236 PBS, while two mock-infected received only PBS diluent (n = 6 infected; n = 2 mock).
237 The females were euthanized and necropsied at 48 hpi (9.5-10.5 dpc). Blood samples
238 were collected prior to euthanasia for post-infection hematological and biochemical
239 analyses. Organs collected for quantification of infectious viral particles and histological
240 analysis included the liver, kidneys, *quadriceps femoris* muscle, ovaries, uterus, placenta
241 and fetus. The same procedures were performed on the remaining pregnant females
242 infected at 13.5–14.5 dpc (n = 7 infected; n = 2 mock), which were necropsied at 48 hpi
243 (15.5-16.5 dpc).

244 - **MAYV WT sexual transmission**

245 To evaluate sexual transmission in both directions, BALB/cJ mice were mated in a 1:1
246 ratio under controlled conditions. For female-to-male transmission, seven 8-week-old
247 females were synchronized in their estrous cycles by exposure to male dirty bedding for
248 72 h prior to mating, as described above, and were infected i.p. with 1 × 10^5 PFU of
249 MAYV in 100 µL of PBS 12 h before pairing with uninfected males. For male-to-female
250 transmission, six synchronized 8-week-old females were paired with males infected i.p.
251 with the same viral dose and schedule. Infected animals were necropsied at 48 hpi,
252 whereas their uninfected partners at 48 h after mating. The liver, spleen, *quadriceps*
253 *femoris* muscle, ovaries, uterus, seminal vesicles, and testes were collected for infectious
254 viral particle detection by plaque assay and for RT-qPCR analysis in organs from exposed

255 animals. Sperm from the bilateral cauda epididymides was collected for plaque assay and
256 RT-qPCR analysis. For analytical purposes, an exposed animal was defined as an
257 uninfected individual mated with an infected partner.

258 **Hematology and biochemistry profile**

259 For hematological analysis, 20 µL of blood per animal were collected and stored in 0.5
260 mL microtubes containing potassium EDTA salts (W anticoagulant, Wiener Lab,
261 Rosario, Argentina) at a 1:10 ratio (EDTA: blood). Samples were analyzed using an Auto
262 Hematology Analyzer BC-5000 Vet (Mindray, Shenzhen, China). The parameters
263 evaluated included white blood cells (WBC), neutrophils (Neu), lymphocytes (Lym),
264 monocytes (Mon), eosinophils (Eos), basophils (Bas), red blood cells (RBC), hemoglobin
265 (HGB), hematocrit (HCT), mean corpuscular volume (MCV), mean corpuscular
266 hemoglobin (MCH), mean corpuscular hemoglobin concentration (MCHC) and platelets
267 (PLT).

268 For biochemical blood profile analysis, 100 µL of whole blood per animal was collected
269 and mixed with 0.5 µL of sodium heparin (Heparin Na, 20 U/mL). Using the Chemistry
270 Analyzer Pointcare® V3 (Tianjin MNCHIP Technologies Co. Ltd, Tianjin, China), the
271 following parameters were evaluated: total protein (TP), albumin (ALB), globulin (GLO),
272 total bilirubin (Tbil), alanine aminotransferase (ALT), aspartate aminotransferase (AST),
273 gamma-glutamyl transferase (GGT), blood urea nitrogen (BUN), and creatinine (CRE).

274 **Tissue collection and processing**

275 Samples collected from each organ of interest were weighed, rapidly frozen in liquid
276 nitrogen under a biosafety cabinet and stored at -70°C until processing. Samples were
277 homogenized using zirconium beads (0.5 mm/tube) and 800 µL of sterile 1× DPBS in a
278 Precellys® 24 homogenizer (Bertin Technologies, France), (2 min, power 10).

279 Homogenates were clarified by centrifugation (6,000 × g, 5 min), and supernatants were
280 stored at −70 °C for viral titration or RT-qPCR analysis.

281 **Viral titration**

282 For viral titration, confluent Vero cell monolayers in 12-well plates (2.6 × 10^6 cells per
283 plate) were inoculated with tissue homogenate–derived supernatants and their 10-fold
284 serial dilutions (200 µL per well) and incubated at 37 °C with 5% CO_2 for 1 h, with gentle
285 rocking every 15 min to ensure uniform inoculum distribution. Mock-infected wells
286 served as negative controls. After adsorption, cells were overlaid with DMEM containing
287 0.8% agarose, 1.6% FBS, penicillin, and streptomycin and incubated for 48 h.
288 Monolayers were then fixed with 4% formaldehyde, stained with crystal violet, and
289 plaques were counted to determine viral titers, expressed as plaque-forming units per
290 gram of tissue (PFU/g).

291 **Mouse sperm collection**

292 The bilateral cauda epididymides were collected in a 60 mm plastic Petri dish and incised
293 with several cuts using fine scissors, releasing the sperm into a 50 µL drop of Dulbecco's
294 Phosphate Buffered Saline 1x (DPBS, Sigma-Aldrich), and stored at −80°C until further
295 processing. Later, sperm samples were thawed and resuspended in 150µL of PBS.
296 Zirconium beads were added to each sample and disruption was performed using a Bullet
297 Blender® STORM 24 (Next Advance Inc., New York, USA) for one minute at speed 8.
298 After centrifugation, 100 µL of supernatant was divided into two aliquots. To assess the
299 presence of MAYV, one aliquot was subjected to cell culture amplification followed by
300 plaque assay, whereas the other was analyzed directly for viral RNA by RT-qPCR.

301 **Viral RNA extraction and detection**

302 Viral RNA from tissues was extracted from clarified tissue homogenate supernatants, as
303 described above, using the QIAamp® Viral RNA Mini Kit (QIAGEN), according to the
304 manufacturer's instructions. RNA from sperm samples was extracted from TRIzol-treated
305 homogenates using the Direct-zol RNA Miniprep Kit (Zymo Research), following the
306 manufacturer's guidelines. RNA samples were eluted in 25µL of nuclease-free water and
307 stored at -80ºC until further use (36). Detection was performed using a one-step real-time
308 reverse transcription PCR (RT-qPCR) assay, employing the primers and probe listed in
309 Table 1, which target an 86-bp region of the MAYV nsP1 gene. Reactions were carried
310 out using TaqMan™ Fast Virus 1-Step Master Mix (Thermo Fisher Scientific) on a
311 QuantStudio™ 7 Pro Real-Time PCR System (Applied Biosystems). Due to limited
312 sample availability, sperm-derived RNA samples were analyzed in technical duplicates.
313 The assay was used for qualitative detection (presence/absence) of viral RNA.

314 **Table 1: primers and probe used for MAYV detection by qPCR.**

MAY-qPCR-Fw	5'-AGGACCCAGAGGAACACTAATA-3'
MAY-qPCR-Rv	5'-CGATACTCTTTCGCCCACTTAC-3'
MAY-qPCR-Probe	5'-/56-FAM/TACCTGCTT/ZEN/CCAGTGGTGTCACAA/3IABkFQ/-3'

315

316 **Cell culture–based isolation of virus from sperm samples**

317 Due to the limited volume of sperm samples, processed samples were subjected to
318 passage in Vero cells to allow potential biological amplification prior to titration. Vero
319 cells were seeded in 96-well plates at 5,000 cells per well in 100 µL of DMEM
320 supplemented with 5% FBS, penicillin (100 U/mL), and streptomycin (100 µg/mL). The
321 following day, cells were inoculated with 100 µL of processed sperm samples. Mock-

322 infected wells receiving culture DMEM alone served as negative controls. After 72 h of
323 incubation at 37 ºC, supernatants were harvested and the presence of infectious viral
324 particles was assessed by plaque assay. Cytopathic effects were monitored using inverted
325 optic microscope Zeiss Primovert, Carl Zeiss Suzhou Co., LTD, China.

326 **Transcriptomics in placenta**

327 For the RNA-seq experiment, three placentas per condition (control uninfected; infected
328 at 7.5-8.5 dpc and infected at 13.5-14.5 dpc) were selected and processed for total RNA
329 extraction. Placentas stored at −80 °C were disrupted in TRI Reagent using a Bullet
330 Blender® STORM 24 (Next Advance Inc., New York, USA) with 0.5 mm zirconium
331 oxide beads (ZROB05, Next Advance Inc.) for 10 min at maximum speed. Following
332 homogenization, the samples were centrifuged to remove beads and debris. The upper
333 aqueous phase was collected and purified using the Direct-zol RNA kit (Zymo Research,
334 USA) according to the manufacturer's instructions. RNA was quantified with RNA HS
335 Qubit (Invitrogen, USA). RNA quality assessment, library construction and sequencing
336 were performed by Macrogen (Seoul, South Korea). Libraries were prepared using
337 TruSeq stranded total RNA with Ribo-Zero Gold kit (Illumina, USA). Sequencing was
338 performed on an Illumina NovaSeq X platform. Paired-end reads of 100 base pairs were
339 obtained.

340 Raw paired-end RNA-seq reads were aligned to the *Mus musculus* reference genome
341 (GRCm39, Ensembl release 114) using STAR v2.7.8a. Aligned reads were quantified at
342 the gene level using featureCounts v2.0.2 (Subread package). The Ensembl GTF
343 annotation file (Mus_musculus.GRCm39.114.gtf) was used.

344 Downstream analysis was conducted in R v4.3.0 using the DESeq2 package. The raw
345 count matrix was filtered to retain genes with a minimum of 10 total reads across all

346 samples. A DESeq2 dataset was constructed with experimental conditions as the main
347 design factor. Variance stabilizing transformation (VST) was applied to normalize data
348 prior to visualization and clustering. Differential expression analyses were performed for
349 multiple contrasts of interest, and log2 fold changes were shrinkage-corrected using the
350 "normal" method of lfcShrink. Genes with an adjusted p-value <0.05 were considered
351 significantly differentially expressed.

352 Volcano plots were generated with ggplot2, where significant genes were highlighted
353 (adjusted p <0.05). Heatmaps of differentially expressed genes were created with
354 pheatmap R package, using variance-stabilized expression values scaled by gene (row-
355 wise z- scores). Color schemes were defined with the RColorBrewer package. Additional
356 hierarchical clustering of differentially expressed genes was performed to assess global
357 expression patterns across experimental groups. Gene ontology analysis was performed
358 using Metascape (37).

359 **Immunohistochemistry**

360 Immediately after the necropsy, placenta and fetus from mid-stage of pregnancy were
361 fixed in 10% neutral buffered formalin (pH 7.4) for further processing. The samples were
362 then decalcified by immersion and agitation in a 3% aqueous nitric acid solution for 24
363 h. Once decalcification was complete, histological processing for paraffin embedding
364 began. Once the paraffin blocks were obtained from each sample, successive 4µm-thick
365 sections were made with a manual rotary microtome (Slee, Germany), and the successive
366 sections were mounted on slides and prepared for immunohistochemistry against MAYV
367 immunoreaction, using a rabbit polyclonal primary antibody (dilution 1:100) according
368 to a previous immunofluorescence protocol developed for immunocytochemistry in cell
369 cultures (38,39). Histological and immunohistochemical blinded examinations were

370 performed using transmitted light microscope (Nikon Eclipse E200®, Nikon Corporation,
371 China) by two different veterinary pathologists.

372 **Data Analysis**

373 Statistical analyses were performed using GraphPad Prism version 10 (GraphPad
374 Software, San Diego, CA, USA). Viral load data (PFU/g) were $\log_{10}$-transformed to
375 approximate a normal distribution. Values below the limit of detection (LOD) were
376 imputed as LOD/2 (630 PFU/g) prior to transformation to enable statistical analysis
377 without introducing bias due to non-detectable values. For viral load analyses, mixed-
378 effects models (REML) were applied with time point, tissue, and/or experimental group
379 as fixed effects, and individual animal as a random effect to account for repeated measures
380 and intra-subject variability. Post hoc comparisons were performed using Tukey's
381 multiple comparisons test. Hematological and biochemical parameters were analyzed
382 using mixed-effects models for repeated measures when longitudinal data were available,
383 with time and/or condition as fixed effects and individual animal as a random effect.
384 When model assumptions were not met, non-parametric tests were applied, including
385 Mann–Whitney U test for two-group comparisons and Kruskal–Wallis test followed by
386 Dunn's multiple comparisons test for multiple groups. Normality of data distributions
387 was assessed using the Shapiro–Wilk test and visual inspection of residuals. RNA-seq
388 differential expression analysis was performed using DESeq2. Genes with fewer than 10
389 total counts across all samples were filtered out. Variance stabilizing transformation
390 (VST) was applied for data normalization prior to visualization and clustering.
391 Differentially expressed genes were identified using adjusted p-values (Benjamini–
392 Hochberg correction), with a significance threshold of adjusted $p < 0.05$. Data are
393 presented as individual values with median lines unless otherwise specified. All statistical
394 tests were two-tailed, and a p value < 0.05 was considered statistically significant.

395 # RESULTS

396 **Bioluminescence reveals rapid dissemination and longitudinal persistence of**
397 **MAYV-nLuc signal.** Luminescence was first detected at 24 hpi (1 dpi) and remained
398 detectable through the predetermined endpoint at 10 dpi. Signals were identified in the
399 forelimbs, hindlimbs, tail, ears, and abdominal region. The abdominal signal decreased
400 after 6 dpi, whereas residual luminescence persisted in peripheral sites, remaining
401 detectable mainly in the limbs at 10 dpi (Fig 2).

402 To assess the presence of infectious virus, plaque assays were performed on tissues
403 collected at 6 and 10 dpi. Infectious viral particles were selectively recovered from the
404 peripheral tissues of 4-week-old mice —including forelimbs, hindlimbs, tail and ears—
405 while visceral organs (liver, spleen, muscle, and kidneys) remained negative. Viral loads
406 in these peripheral compartments spanned nearly two orders of magnitude, ranging from
407 3.17 to 5.47 $\log_{10}$ PFU/g (1.49×10^3 to 2.98×10^5 PFU/g), with the highest titers detected in
408 tail and limb samples. In contrast, tissues from 8-week-old animals that exhibited
409 luminescent signals *in vivo* did not yield detectable infectious virus. This apparent
410 discrepancy may be attributable to differences in analytical sensitivity between reporter-
411 based imaging and plaque assays, the latter of which requires a minimum threshold of
412 viable, replication-competent virions.

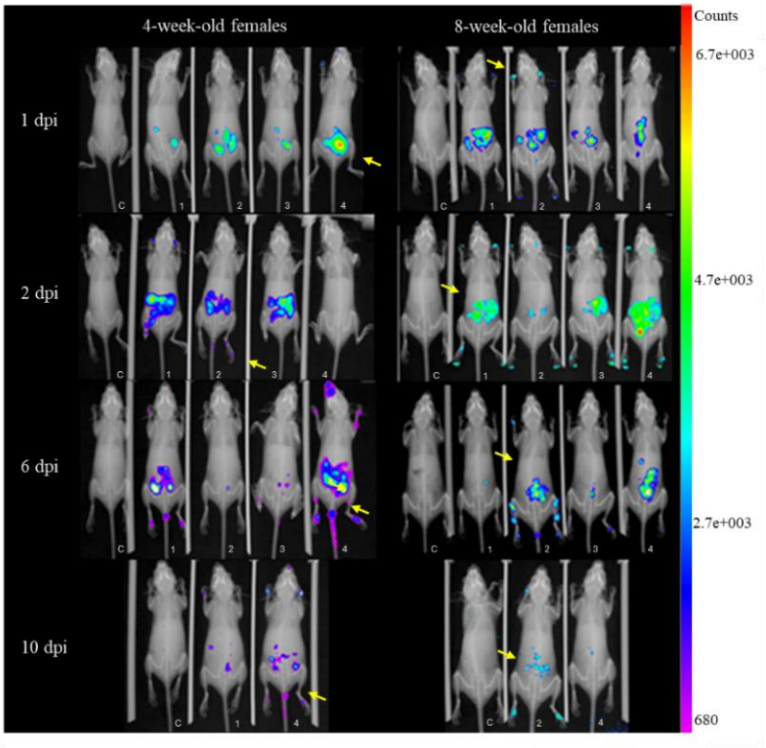

Figure 2. *In vivo* bioluminescence imaging of MAYV-nLuc infection in females at 4 and 8 weeks-old following i.p. inoculation (representative image). Luminescent signals (yellow arrows) were detected in the limbs, tail, ears, and abdominal region at 1 (24 hpi), 2 (48 hpi), 6 and 10 dpi. Abdominal signals declined after 6 dpi, whereas residual luminescence persisted mainly in the limbs at later time points. Images from all animals in each age group are shown. All images were acquired and displayed using identical exposure settings and a fixed color scale to enable direct comparisons over time. C, mock-infected control.

Temporal dynamics and tissue tropism of MAYV infection in 4-week-old mice. Viral titers exhibited time- and tissue-dependent differences during acute infection (Fig 3A). Mixed-effects analysis with Tukey's multiple comparisons identified a significant increase in seminal vesicles at 48 hpi compared with 24 hpi (Mean difference = 0.9452, SE of difference = 0.3397, p = 0.0284). Model-based estimates are reported as mean differences (± SE), while graphical representations show individual values with median lines due to non-normal data distribution. At 24 hpi, no significant inter-tissue differences were detected, consistent with a relatively homogeneous early dissemination pattern. By

48 hpi, tissue-specific differences emerged, with spleen titers exceeding those in liver (Mean difference = 0.8391, SE of difference = 0.2150, p = 0.0352) and muscle (Mean difference = 1.257, SE of difference = 0.2840, p = 0.0156). This substantial difference suggests the spleen as a primary site of viral accumulation compared to muscular tissue Sex-based analyses revealed transient differences at 24 hpi (Fig 3B). Specifically, significant female–male differences were observed in the spleen (mean difference = 1.593, SE of difference = 0.5278, p = 0.0109) and kidneys (mean difference = 2.038, SE of difference = 0.4765, p = 0.0159). In both tissues, males exhibited substantially higher viral titers than females at this time point. Organ-specific viral distribution also varied within each sex at 24 hpi. Among females, viral loads in the kidneys were significantly higher than in the muscle (mean difference = 1.078, SE of difference = 0.2911, p = 0.0493). Conversely, in males, the spleen showed a significantly greater viral burden compared to the liver (mean difference = 0.5601, SE of difference = 0.1205, p = 0.0205). By 48 hpi, no significant differences in viral loads were observed either between sexes or among tissues within each sex (Fig 3C). This lack of statistical significance ($p > 0.05$ for all comparisons) indicates that the early sex-dependent effects and tissue-specific disparities observed at 24 hpi are not sustained as the infection progresses toward later stages.

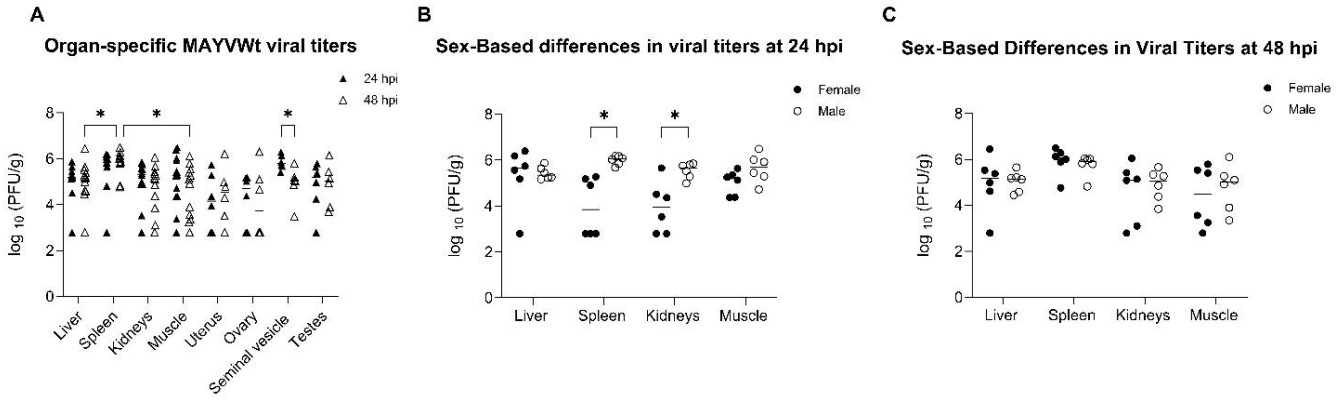

Figure 3. Early systemic dissemination with time-dependent tissue tropism and transient sex effects.

449 Viral loads (log_{10} PFU/g) across tissues at 24 and 48 hours post-infection (hpi) and sex-based comparisons
450 at each time point. (A) Viral loads across tissues at 24 and 48 hpi. (B) Sex-based comparison of viral loads
451 across tissues at 24 hpi. (C) Sex-based comparison at 48 hpi. Viral loads were analyzed using mixed-effects
452 models (REML) with time point and tissue as fixed effects and individual animal as a random effect,
453 followed by Tukey's multiple comparisons test. Values below the limit of detection were assigned a value
454 of LOD/2 (630 PFU/g) prior to transformation. Each dot represents an individual animal; horizontal lines
455 indicate median values. Only statistically significant comparisons are indicated. Statistical significance was
456 defined as $p < 0.05$ (*), $p < 0.01$ (**) and $p < 0.001$ (***).

457 **Early hematological alterations during acute MAYV infection.** Hematological
458 analysis revealed alterations in leukocyte profiles during acute infection. Total white
459 blood cell counts (WBC) decreased at 24 and 48 hpi, accompanied by increased
460 neutrophil (NEU) and decreased lymphocyte (LYM) percentages (Fig 4A–C). Platelet
461 counts (PLT) also decreased at both time points (Fig 4D). Eosinophils (EOS) decreased,
462 basophils (BAS) increased at 48 hpi, and monocytes (MON) remained stable in infected
463 animals but decreased in mock controls (Fig S1A–C). Red blood cell counts (RBC)
464 increased at 48 hpi, while hemoglobin (HGB) and hematocrit (HCT) increased at both
465 time points (Fig S1D–F). Mean corpuscular volume (MCV) increased at 24 and 48 hpi,
466 mean corpuscular hemoglobin (MCH) increased at 24 hpi, and mean corpuscular
467 hemoglobin concentration (MCHC) remained unchanged (Fig S3A–C). Red cell
468 distribution width (RDW-CV and RDW-SD) decreased at both time points. Mean platelet
469 volume (MPV) increased, while platelet distribution width (PDW) decreased at 48 hpi.
470 Procalcitonin (PCT) decreased in infected animals without changes in mock controls (Fig
471 S3D–H). Statistically significant differences are indicated in the corresponding figures.

472 **Biochemical and metabolic parameters.** Aspartate transaminase (AST) at both 24 and
473 48 hpi and increased alanine transaminase (ALT) at 48 hpi (Fig 4E–F). Creatinine (CRE)
474 remained stable, whereas blood urea nitrogen (BUN) decreased at 24 hpi and showed a

475 decreasing trend at 48 hpi, including in mock animals (Fig S1G–H). Total protein (TP)
476 decreased at 48 hpi, while albumin (ALB), globulin (GLO), and gamma-glutamyl
477 transferase (GGT) remained unchanged (Fig S2A–C, E). Total bilirubin (TBIL) decreased
478 at 24 hpi (Fig S2D). Glucose (GLU) increased at both time points, and body weight (BW)
479 decreased at 24 and 48 hpi (Fig S2G–H). Statistical significance is indicated in the
480 corresponding figures.

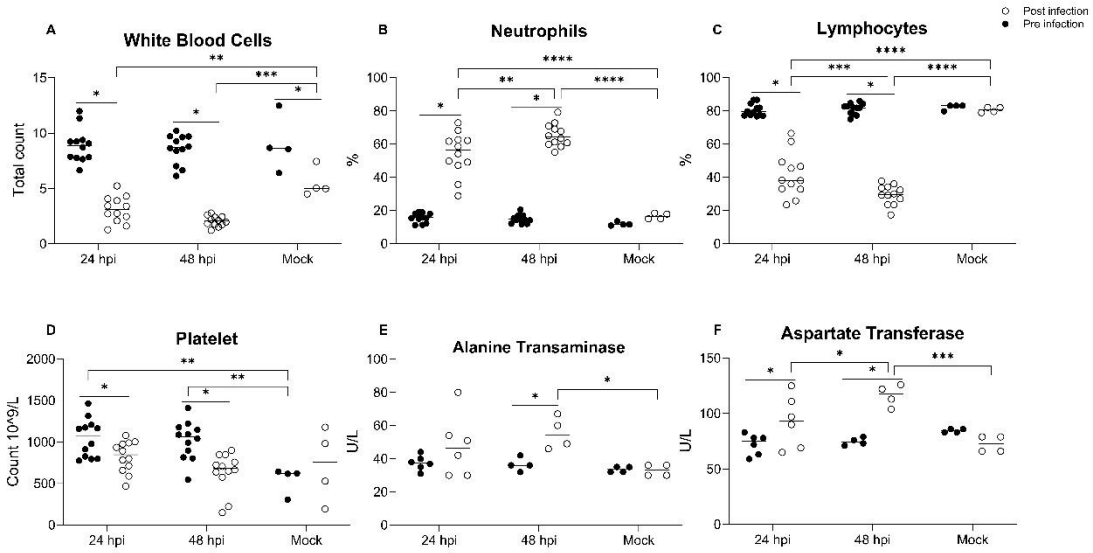

481

482 **Figure 4. Early hematological and hepatic changes following acute MAYV infection.**
483 Hematological and hepatic parameters during acute MAYV infection at 24 and 48 hours post-infection
484 (hpi) compared with mock controls. (A) Total white blood cell (WBC) count, (B) neutrophil percentage
485 (NEU), (C) lymphocyte percentage (LYM), (D) platelet count (PLT), (E) alanine transaminase (ALT), and
486 (F) aspartate transaminase (AST). Each dot represents an individual animal; horizontal lines indicate
487 median values. Statistical analyses were performed using mixed-effects models (REML) for repeated
488 measures with time and condition as fixed effects and individual animal as a random effect, or non-
489 parametric tests when assumptions were not met. Differences were considered statistically significant at p
490 < 0.05 (*), $p < 0.01$ (**) and $p < 0.001$ (***).

491 **Gestational stage–dependent differences in MAYV distribution during pregnancy.**
492 At 48 hpi, viral titers exhibited significant variations based on gestational stage across

493 multiple tissues (Fig 5). Mixed-effects modeling followed by Tukey's multiple
494 comparison test revealed significantly higher infectious viral loads at 48 hpi in tissues
495 analyzed at 15.5–16.5 dpc (pregnant mice infected at 13.5-14.5 dpc) compared with those
496 analyzed at 9.5–10.5 dpc (pregnant mice infected at 7.5-8.5 dpc). This stage-dependent
497 increase was observed in the spleen (mean difference = 0.5751, SE of difference =
498 0.1624, p = 0.0213), liver (mean difference = 1.924, SE of difference = 0.1552, p =
499 0.0011), kidneys (mean difference = 1.691, SE of difference = 0.3097, p = 0.0055), uterus
500 (mean difference = 1.660, SE of difference = 0.6606, p = 0.0403) and placenta (mean
501 difference = 0.7328, SE of difference = 0.2277, p = 0.0061). However, infectious virus
502 remained undetectable in fetal tissues at this same stage (15.5–16.5 dpc), with titers
503 falling below the limit of detection. This suggests that even when the placenta is
504 significantly infected, the virus remained undetectable at the fetal compartment in an
505 infectious form. Within early gestation (9.5–10.5 dpc), tissue-specific differences were
506 observed, with the spleen showing higher titers than the liver and kidneys. At mid-
507 gestation, infectious viral particles remained detectable in maternal and placental
508 compartments, supporting ongoing systemic dissemination despite restricted recovery of
509 infectious virus from fetuses.

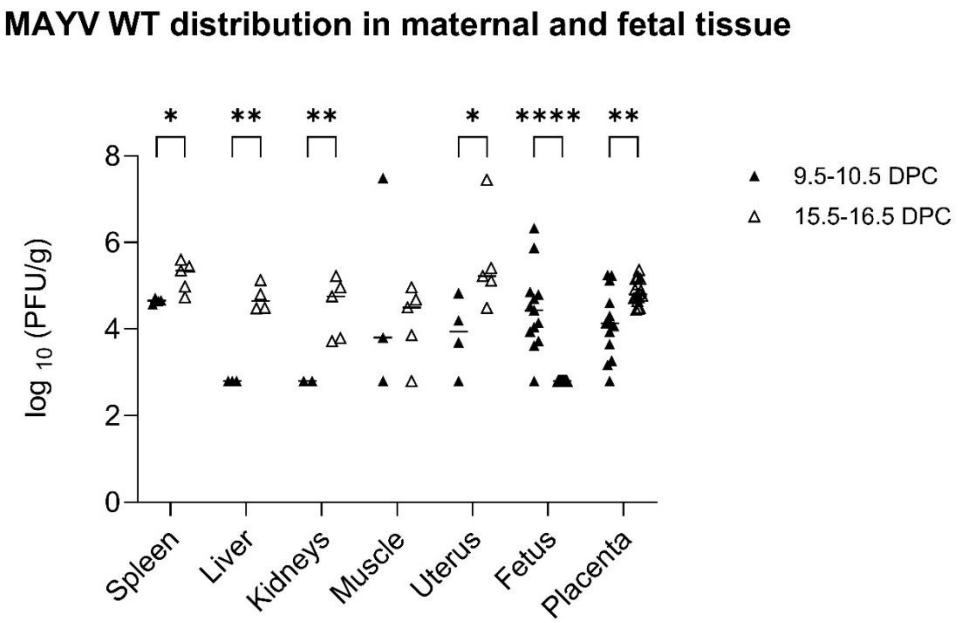

Figure 5. Gestational stage shapes maternal–fetal distribution and restricts recovery of infectious virus from mid-gestation fetuses. Infectious viral loads (log_{10} PFU/g) in maternal and fetal tissues at 48 hours post-infection (hpi) according to gestational stage. Females were infected at early (7.5–8.5 dpc; analyzed at 9.5–10.5 dpc) or mid-gestation (13.5–14.5 dpc; analyzed at 15.5–16.5 dpc). Each dot represents an individual animal; horizontal lines indicate median values. Viral loads were analyzed using mixed-effects models (REML) with gestational stage and tissue as fixed effects and individual animal as a random effect, followed by Tukey's multiple comparisons test. Values below the limit of detection were assigned a value of LOD/2 (630 PFU/g) prior to transformation. Only statistically significant comparisons are indicated. Only statistically significant comparisons are indicated. Statistical significance was defined as $p < 0.05$ (*), $p < 0.01$ (**) and $p < 0.001$ (***).

Acute MAYV infection induces leukocyte redistribution without overt hematological cytopenias at 48 hpi. Infected females at both gestational stages exhibited a shift in leukocyte distribution, characterized by increased neutrophil and decreased lymphocyte percentages compared with mock controls (Fig S4A–B). Total white blood cell counts (WBC) did not differ between infected and mock animals (Fig S4C), indicating leukocyte redistribution rather than overall leukocytosis. Red blood cell counts, platelet numbers, and procalcitonin levels remained comparable between groups (Fig

528 S4D–F). Given the limited mock sample size, these findings should be interpreted with
529 caution.

530 **Immunohistochemistry confirms placental and fetal localization of MAYV at mid**
531 **stage.** Immunohistochemical analysis revealed clear differences in MAYV antigen
532 distribution between infected and non-infected tissue at fetus and placenta from an
533 infected female at mid-gestation. In placentas from infected females, moderate granular
534 cytoplasmic staining was observed, marking a substantial proportion of the giant
535 trophoblast cells within the maternal–fetal junction zone (basal plate) indicating focal
536 placental infection. In contrast, placentas from non-infected pregnant females showed
537 only nonspecific erythrocyte staining and overall negative to mild background labeling.
538 In fetus from infected female, intense immunostaining was detected across multiple
539 organs, particularly in the visceral epithelium of the intestine, the developing bone
540 (growth cartilage), and other collagen-rich tissues including cartilage and dermis.
541 Calcified bone exhibited no staining or only minimal labeling in both intensity and extent.
542 Fetuses from non-infected females were largely negative, with nonspecific erythrocyte
543 staining and minimal background labeling in collagen-rich tissues (Fig 6). This discrepancy
544 may reflect detection limits of plaque assays or persistence of viral antigens following partial viral
545 clearance.

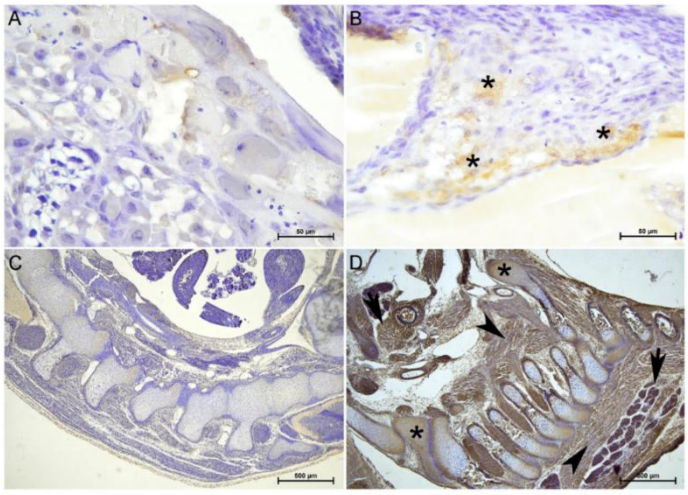

Figure 6. IHC against MAYV. A) Placenta of an uninfected mouse (control): Negative to mild (-/+) immunostaining of isolated trophoblasts (foam giant cells) from the basal plate of the maternal-fetal junction is observed. Scale bar = 50µm, 40×. B) Placenta of an experimentally infected mouse: Mild to moderate, granular intracytoplasmic staining of foci of trophoblasts (foam giant cells) from the basal plate of the maternal-fetal junction is observed (asterisks). Scale bar = 50µm, 40×. C) Fetus of the same uninfected mouse of Figure A: No immunostaining against MAYV is observed (-). Scale bar = 500µm, 4×. D) Fetus of the same experimentally infected mouse of Figure B: There is intense immunostaining in several organs, particularly in uncalcified developing bone and growth cartilage (asterisks), as well as other collagen-rich tissues (cartilage and dermis) (arrowheads) and the perimysium of skeletal muscles (arrows). Already calcified bone shows no staining or minimal staining in intensity and extent. Scale bar = 500µm, 4×.

Placental transcriptional responses to MAYV are gestational stage-dependent. To investigate placental transcriptional responses to MAYV infection, differential gene expression was performed. The profiles revealed gene expression patterns influenced by viral infection at early and mid-stages: 208 genes were upregulated and 60 downregulated at the early stage, and 139 genes were upregulated and 1 downregulated at the mid stage (Fig 7A and Table S1). Among the upregulated genes, 50 were shared between both stages, leaving 158 stage-specific upregulated genes at the early stage and 89 at the mid stage. These data suggest a robust transcriptional response to infection during the early

566 stage of pregnancy, while the response in mid pregnancy, although sharing common
567 pathways, is comparatively attenuated.

568 Gene Ontology (GO) enrichment analysis of the 50 shared upregulated genes revealed
569 significant association with antiviral defense pathways, including responses to viral
570 infection, interferon-stimulated genes (ISGs) activity and cytokine-mediated signaling
571 (Fig 7B).

572 The 158 genes uniquely upregulated in the early stage were enriched not only for the
573 immune pathways but also for distinct biological processes, including heart development,
574 myeloid cell development, regulation of plasminogen activation, connective tissue
575 development, and adipogenesis (Fig 7C). In contrast, the 89 late-stage-specific
576 upregulated genes were again predominantly associated with immune functions,
577 specifically type II interferon signaling, negative regulation of innate immune response,
578 and innate antiviral immune response (Fig 7D).

579 Finally, GO analysis of the 60 genes downregulated specifically at the early stage
580 identified enrichment for processes such as multi-organism reproductive process, antigen
581 processing and presentation of peptide antigen via MHC class I, lymphocyte activation,
582 signaling by NTRKs, insulin secretion, thermogenesis, extracellular matrix organization,
583 and adrenergic signaling in cardiomyocytes (Fig 7E).

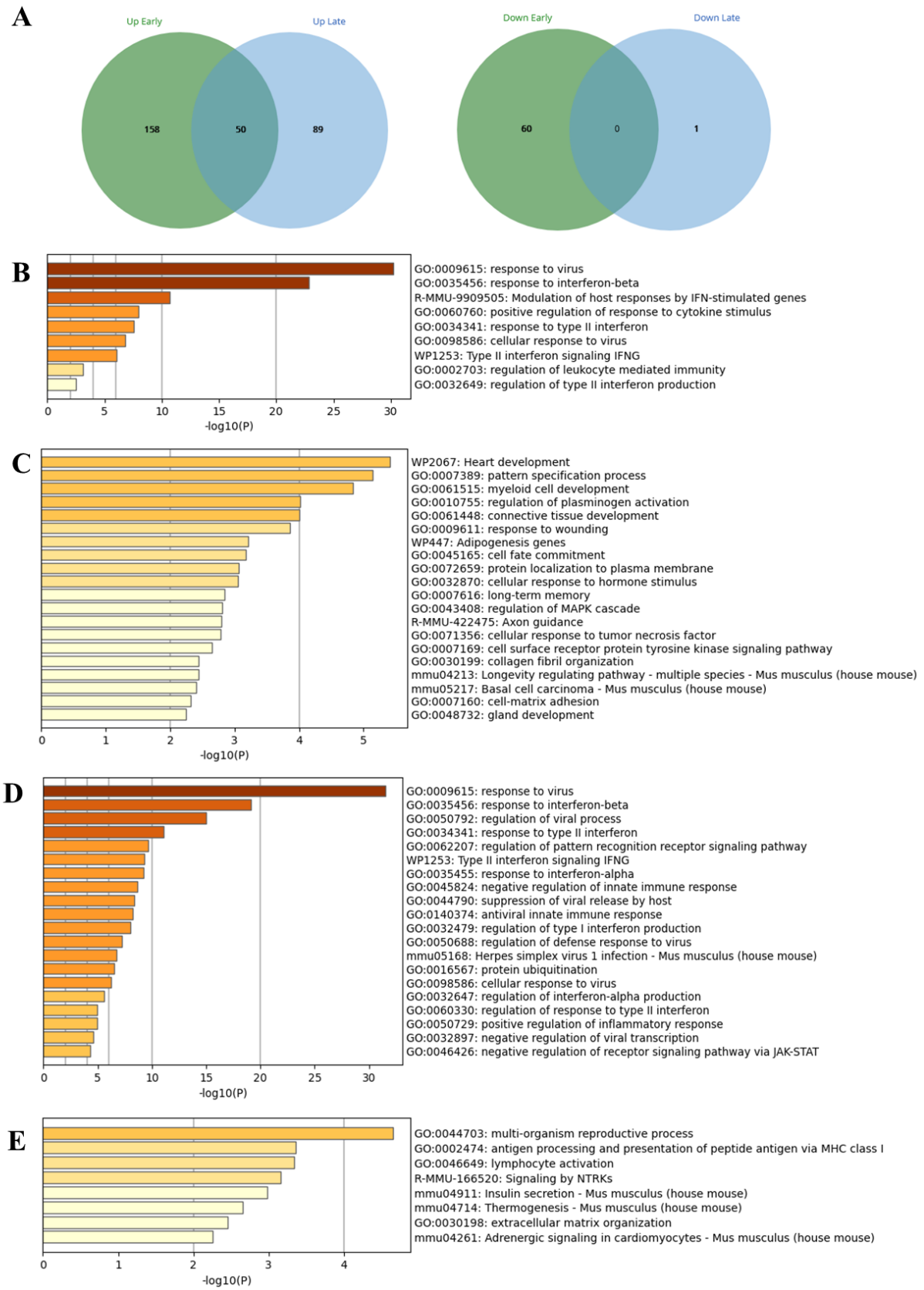

Figure 7. Transcriptomic profiles and Gene Ontology enrichment of placental response to MAYV infection at early and mid-gestational stages. A) Comparison of placentas infected at 7.5–8.5 dpc (early)

587 and 13.5–14.5 dpc (mid) versus controls revealed 208 up-/60 down-regulated genes at early stage and 139
588 up-/1 down-regulated at mid stage, with 50 genes shared between stages. B) Shared genes were enriched
589 for antiviral and interferon-mediated responses. C) Early-stage-specific genes were associated with
590 immune, developmental, and metabolic pathways. D) Mid-stage-specific genes were mainly related to type
591 II interferon and innate immune modulation. E) Early-stage down-regulated genes were enriched for
592 reproductive, metabolic, and signaling processes.

593 **MAYV detection in reproductive tissues and sperm.** Following mating, the liver,
594 spleen, *quadriceps femoris* muscle, ovaries, uterus, seminal vesicles and testes were
595 analyzed for the presence/absence of MAYV by plaque assay in all animals. RT-qPCR
596 was performed on the spleen of infected animals and on the corresponding organs from
597 exposed animals. To detect the presence/absence of MAYV in sperm, RT-qPCR was
598 performed and, following cell culture amplification and plaque assay.

599 Infectious viral particles were detected in the spleen (7/7), ovaries (3/7), and muscle (1/7)
600 of infected females mated with uninfected males. In contrast, all organs analyzed from
601 exposed males were negative by both plaque assay and RT-qPCR. However, after cell
602 culture amplification of sperm samples followed by plaque assay, infectious virus was
603 detected in one exposed male (1/7), which had been paired with the female positive for
604 infectious virus in both the spleen and muscle.

605 In infected males mated with uninfected females, infectious viral particles were
606 consistently detected in the testes (6/6) and in the spleen (3/6). Plaque assays performed
607 after cell culture amplification of sperm revealed infectious virus in four males (4/6),
608 consistent with the cytopathic effect observed (Fig 8). Viral RNA was also detected by
609 RT-qPCR in direct unamplified sperm samples from the same four animals. No infectious
610 virus was detected in the seminal vesicles. Among exposed females, infectious viral

611 particles tested positive in two animals: the uterus and ovary of one female and the spleen
612 of another, although the RT-qPCR resulted below the limit of detection.

613 Overall, viral detection in exposed animals was limited and inconsistent across analytical
614 approaches.

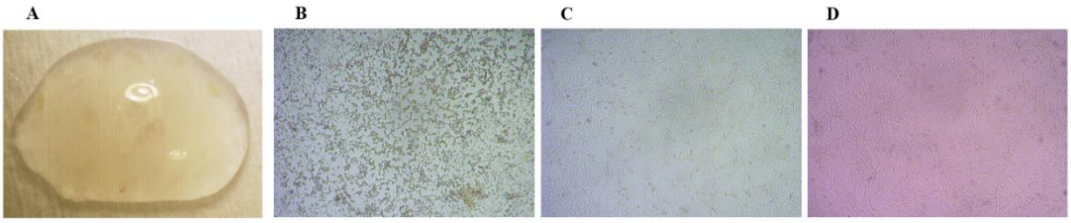

615

616 **Figure 8. Cytopathic effect of MAYV in sperm cell culture–based amplification** (Representative image).
617 (A) Sperm extracted from the bilateral cauda epididymides. (B´D) Representative images of Vero cells
618 inoculated with processed sperm samples showing a MAYV-positive sample (B) a MAYV-negative sample
619 (C) and Mock-infected Vero cells (D). Cell morphology was examined by a Zeiss Primovert inverted light
620 microscope (40×).

621

622 DISCUSSION

623 Elucidating the tissue tropism and viral dynamics of MAYV is essential given the limited
624 evidence available for this emerging arbovirus and the relevance of murine models for
625 characterizing infection *in vivo*. Here, we provide evidence of MAYV dissemination to
626 fetal tissues in mice, identifying anatomical targets not previously described. Together,
627 these findings support a model in which gestational timing critically determines placental
628 permissiveness and fetal exposure to MAYV, identifying early gestation as a window of
629 heightened vulnerability during acute infection. Although direct temporal equivalence
630 between murine and human gestation is not possible, early murine gestation (7.5-8.5 dpc)
631 represents a developmental window of active placentation and early organogenesis that

632 broadly parallels the first trimester of human pregnancy, whereas mid-gestation (13.5-
633 14.5 dpc) reflects a more mature placental interface (21,40). Considering that related
634 alphaviruses may cross the placental barrier, our results underscore the importance of
635 including pregnancy models when assessing MAYV transmission routes (41).

636 To examine early dissemination under controlled conditions, we employed a
637 nanoluciferase-expressing MAYV reporter to evaluate intraperitoneal delivery as a
638 strategy to achieve systemic exposure. *In vivo* imaging showed rapid and sustained viral
639 spread, with peripheral luminescent patterns consistent with the musculoskeletal
640 involvement previously described in experimental models and human disease (18,25,29).

641 The incomplete overlap between bioluminescent signal and recovery of infectious virus,
642 particularly in older animals, likely reflects differences in analytical sensitivity between
643 reporter detection and plaque assays or the persistence of viral material following
644 clearance of replicative particles. In contrast, the consistent recovery of infectious virus
645 in younger mice supports age-dependent variation in susceptibility and viral maintenance
646 within target tissues.

647 This imaging approach enabled longitudinal, non-invasive monitoring of viral dynamics
648 over a 10-day period, encompassing both acute infection and early recovery phases
649 (25,26). By providing temporal and anatomical resolution of dissemination events that
650 are difficult to capture in natural transmission settings, the model links viral spread to
651 measurable tissue outcomes.

652 Together, these observations expand the experimental landscape for MAYV research,
653 supporting mechanistic investigations of tissue tropism, host responses, and transmission
654 potential under standardized conditions, and offering a framework for future studies
655 addressing reproductive involvement and non-vector routes of spread.

656 MAYV WT exhibited rapid and systemic dissemination at 24 and 48 hpi, with infectious
657 virus detected across multiple organs, including detection in reproductive tissues of
658 pregnant females. These results are consistent with other murine alphavirus models,
659 including IFNAR−/− mice, in which widespread viral detection at early time points
660 reflects acute viremia (28). This pattern reflects an initial homogeneous dissemination
661 phase at 24 hpi followed by the emergence of tissue-specific viral accumulation at 48 hpi,
662 consistent with previous murine MAYV models showing that viral burden is influenced
663 by host age, immune status, and route of infection, with predominant viral accumulation
664 in skeletal muscle, limbs, and lymphoid organs such as the spleen (10,30). Infectious
665 particles were also detected in muscle, supporting the myopathy and myositis previously
666 described during MAYV infection (10,29). The increase in viral load in seminal vesicles
667 at 48 hpi further supports progressive involvement of reproductive tissues during acute
668 infection, consistent with the detection of infectious virus in male reproductive organs.

669 The early hematological alterations observed in our study partially align with previous
670 experimental and clinical reports of MAYV infection. In IFNAR−/− mice model, early
671 leukopenia predominantly driven by lymphopenia was reported during acute infection
672 (29), consistent with the leukopenia and lymphocyte reduction detected in our model. In
673 contrast, a BALB/c intraplantar infection model described increases in monocytes,
674 neutrophils, and lymphocytes during the acute phase (25), indicating that hematological
675 profiles may vary depending on experimental conditions. In human cases, leukopenia,
676 thrombocytopenia, and elevated ALT and AST have been documented among reported
677 laboratory abnormalities (18), which parallels the transient cytopenias and
678 aminotransferase elevations observed here. Together, these comparisons suggest that
679 early systemic hematological and biochemical changes are reproducible features of
680 MAYV infection, although their magnitude and direction may differ across models and

681 clinical settings. Despite the limited mock sample size in pregnant cohorts, the consistent
682 leukocyte redistribution observed at 48 hpi across gestational stages supports the
683 interpretation of an early systemic inflammatory response rather than global
684 hematological impairment.

685 MAYV belongs to the Alphavirus genus (18,30), which includes viruses capable of
686 affecting the nervous system and embryonic development. The detection of infectious
687 particles in reproductive organs (uterus, ovary, testes, seminal vesicles) at both time
688 points highlights a tissue tropism previously described in immunodeficient mice (15) and
689 raises the possibility of sexual or vertical transmission. Transient and early sex-based
690 differences were observed at 24 hpi. These differences were no longer evident at 48 hpi.
691 While most studies focused on age and nutritional status as determinants of disease
692 outcome (25,31,42), these observations suggest a potential sex-dependent component of
693 MAYV infection that warrants further investigation, particularly given similar findings
694 reported for CHIKV (43).

695 A gestational stage–dependent susceptibility was evident in our model. At the early stage
696 of pregnancy (7.5–8.5 dpc infection; analyzed at 9.5–10.5 dpc), fetuses contained
697 infectious particles at 48 hpi, indicating that MAYV can cross the maternal–fetal barrier
698 during acute infection. In contrast, our data suggest a more restrictive placental
699 environment during mid-gestation (13.5–14.5 dpc; analyzed at 15.5–16.5 dpc), as no
700 infectious particles were recovered from fetal tissues despite significant placental viral
701 loads. It is critical to interpret this 'restriction' specifically as the absence of infectious
702 viral particles detectable by plaque assay. While this confirms a lack of replication-
703 competent virions in the fetus at this stage, it does not preclude the potential presence of
704 viral RNA or non-infectious antigens that might be detectable through more sensitive

705 molecular methods. This is supported by our immunohistochemistry results, where viral
706 antigen was detected in fetal tissues at mid-gestation despite the absence of recoverable
707 infectious virus, suggesting either focal infection below the limit of detection or the
708 persistence of viral antigens following partial viral clearance. This timing-dependent
709 susceptibility is consistent with observations from ZIKV infection, where placental
710 infection and transplacental transmission are strongly associated with maternal infection
711 occurring during the first trimester of human pregnancy, whereas infections acquired at
712 later gestational stages are less frequently linked to fetal exposure (20,44). This
713 window—analogous to early human embryogenesis (41)— displayed a broad
714 transcriptional response (208 upregulated, 60 downregulated genes), including alterations
715 in developmental and tissue-remodeling programs, as well as downregulation of
716 hormonal signaling, MHC I presentation, and ECM organization. These disruptions are
717 compatible with teratogenesis described for alphaviruses such as Semliki Forest virus
718 (42) and ZIKV (21).

719 In contrast, at mid-gestation infection (13.5–14.5 dpc), infectious viral particles were not
720 detected in fetuses, and transcriptional activation was more restricted (139 upregulated, 1
721 downregulated), dominated by interferon-mediated pathways. This profile aligns with
722 increased placental maturity and antiviral competence (21). The presence of infectious
723 viruses in placenta and uterus, but not in fetal tissues, supports restricted fetal infection at
724 this stage (40,41). Together, these findings support the concept of a conserved gestational
725 window of vulnerability to vertical transmission among arboviruses, in which early
726 placentation is associated with increased permissiveness at the maternal–fetal interface.
727 The 50 shared upregulated genes across gestational stages—mostly ISGs—reflect a
728 conserved antiviral signature, but timing-dependent transcriptional divergence
729 underscores critical periods of vulnerability, including disruption of angiogenic and

730 developmental pathways (45) and inflammatory responses characteristic of MAYV
731 (25,26). Viral antigen was detected by immunohistochemistry in placental and fetal
732 tissues at mid-gestation, despite the absence of recoverable infectious virus, suggesting
733 focal or low-level infection below plaque assay detection limits or persistence of viral
734 antigens following partial viral clearance.

735 While direct extrapolation from murine models to humans is limited, these findings
736 provide a biologically plausible framework to explore potential maternal–fetal risks with
737 MAYV infection in human during pregnancy.

738 Limitations should be considered when interpreting these findings. Intraperitoneal
739 inoculation does not fully recapitulate natural mosquito-borne transmission and may
740 influence early viral kinetics. However, this route is widely used in murine models of
741 systemic arbovirus infection and was deliberately selected to enable controlled
742 assessment of early systemic dissemination and tissue tropism while minimizing
743 procedure-related distress (46,47) and local inflammatory confounders. Although
744 intraplantar models better reproduce articular manifestations (25,26,28), intraperitoneal
745 delivery provides a standardized framework to evaluate systemic viral dynamics.

746 Previous murine studies have reported systemic MAYV dissemination and detection of
747 viral RNA in gonadal tissues, suggesting broader tissue distribution (48), although
748 evidence supporting a functional role of reproductive infection in transmission has
749 remained indirect. In the present study, infectious virus was detected in reproductive
750 organs and sperm, supporting the biological plausibility of sexual transmission, though
751 not establishing it as an efficient route and therefore requiring dedicated follow-up
752 studies. Detection among exposed animals was infrequent, consistent with minimal or
753 transient exposure rather than sustained transmission. If sexual transmission occurs, it is

754 likely to involve low-level infection and restricted replication within gonadal tissues,
755 potentially limiting detectability and contributing to the scarcity of documented cases, a
756 challenge also described for other arboviruses in semen (41).

757 Taken together, these findings broaden the understanding of MAYV pathogenesis by
758 integrating virological, transcriptomic, histological, and imaging approaches within a
759 unified murine model. We provide evidence of expanded tissue tropism, including
760 reproductive and fetal involvement, and identify gestational timing as a determinant of
761 placental permissiveness and fetal exposure. Detection of infectious virus in reproductive
762 tissues supports the biological plausibility of non-vector transmission, although its
763 epidemiological relevance remains uncertain. While extrapolation to humans requires
764 caution, these results establish a preclinical framework for investigating MAYV systemic
765 dissemination, maternal–fetal infection, and potential transmission routes.

766

767 # CONCLUSION

768 This study establishes a murine model of MAYV infection that reveals rapid systemic
769 dissemination followed by tissue-specific viral distribution, broad tissue tropism, and
770 early involvement of reproductive organs. Transient sex-dependent differences were
771 observed during the early phase of infection, suggesting a potential but limited role of sex
772 in modulating viral dynamics. Gestational stage emerged as a key determinant of
773 outcomes: specifically, infection initiated during early pregnancy (7.5–8.5 dpc) and
774 analyzed at 9.5–10.5 dpc identified a window of increased susceptibility associated with
775 the detection of infectious viral loads in fetal tissue. In contrast, infection occurring during
776 mid-gestation (13.5–14.5 dpc) and analyzed at 15.5–16.5 dpc was associated with

restricted fetal infection despite sustained viral presence in maternal and placental tissues. The detection of infectious viral particles in reproductive tissues supports the biological plausibility of alternative transmission routes, although their epidemiological relevance remains uncertain. These findings provide a comprehensive experimental framework to advance the understanding of MAYV pathogenesis, systemic dissemination, and maternal–fetal and non-vector transmission dynamics.

REFERENCES

1. Organización Panamericana de la Salud, Organización Mundial de la Salud. Alerta epidemiológica: fiebre de Mayaro. Washington (DC): OPS/OMS; 2019. Available from: https://www.paho.org

2. Blohm G, Elbadry MA, Mavian C, Stephenson C, Loeb J, White S, et al. Mayaro as a Caribbean traveler: evidence for multiple introductions and transmission of the virus into Haiti. Int J Infect Dis. 2019;87:151–153. doi:10.1016/j.ijid.2019.07.031

3. Ganjian N, Riviere-Cinnamond A. Mayaro virus in Latin America and the Caribbean. Rev Panam Salud Publica. 2020;44:e14. doi:10.26633/RPSP.2020.14

4. Valencia-Marín BS, Gandica ID, Aguirre-Obando OA. The Mayaro virus and its potential epidemiological consequences in Colombia: an exploratory biomathematics analysis. Parasit Vectors. 2020;13(1):519. doi:10.1186/s13071-020-04354-1

5. Brustolin M, Bartholomeeusen K, Rezende T, Ariën KK, Müller R. Mayaro virus, a potential threat for Europe: vector competence of autochthonous

800 vector species. Parasit Vectors. 2024;17(1):93. doi:10.1186/s13071-024-
801 06293-7

802 6. Celone M, Beeman S, Han BA, Potter AM, Pecor DB, Okech B, et al.
803 Understanding transmission risk and predicting environmental suitability
804 for Mayaro virus in Central and South America. PLoS Negl Trop Dis.
805 2024;18(1):e0011859. doi:10.1371/journal.pntd.0011859

806 7. García-Romero C, Carrillo Bilbao GA, Navarro JC, Martin-Solano S,
807 Saegerman C. Arboviruses in mammals in the Neotropics: a systematic
808 review. Viruses. 2023;15(2):417. doi:10.3390/v15020417

809 8. Fundación iO. Aumento significativo de casos de fiebre Mayaro en Acre,
810 Brasil. 2025. Available from: https://fundacionio.com/aumento-
811 significativo-de-casos-de-fiebre-mayaro-en-acre-brasil/

812 9. Andreolla AP, Borges AA, Bordignon J, Duarte dos Santos CN. Mayaro
813 virus: the state of the art for antiviral drug development. Viruses.
814 2022;14(8):1787. doi:10.3390/v14081787

815 10. Diagne CT, Bengue M, Choumet V, Hamel R, Pompon J, Missé D. Mayaro
816 virus pathogenesis and transmission mechanisms. Pathogens.
817 2020;9(9):738. doi:10.3390/pathogens9090738

818 11. Marinho MS, Ferreira GM, Grosche VR, Nicolau-Junior N, Campos TL,
819 Santos IA, et al. Evolutionary profile of Mayaro virus in the Americas: an
820 update into genome variability. Viruses. 2024;16(5):809.
821 doi:10.3390/v16050809

822 12. Cereghino C, Roesch F, Carrau L, Hardy A, Ribeiro-Filho HV, Henrion-
823 Lacritick A, et al. The E2 glycoprotein holds key residues for Mayaro virus
824 adaptation to the urban Aedes aegypti mosquito. PLoS Pathog.
825 2023;19(4):e1010491. doi:10.1371/journal.ppat.1010491

826 13. Mendonça DC, Reis EVS, Arias NEC, Valencia HJ, Bonjardim CA. A study
827 of the MAYV replication cycle: correlation between the kinetics of viral
828 multiplication and viral morphogenesis. Virus Res. 2022;323:199002.
829 doi:10.1016/j.virusres.2022.199002

830 14. Ribeiro-Filho HV, Coimbra LD, Cassago A, Rocha RPF, Guerra JVS, de
831 Felicio R, et al. Cryo-EM structure of the mature and infective Mayaro virus
832 at 4.4 Å resolution reveals features of arthritogenic alphaviruses. Nat
833 Commun. 2021;12(1):3038. doi:10.1038/s41467-021-23400-9

834 15. Krokovsky L, Lins CRB, Guedes DRD, Wallau GL, Ayres CFJ, Paiva
835 MHS. Dynamics of Mayaro virus transmission in Aedes aegypti, Culex
836 quinquefasciatus mosquitoes, and a mouse model. Viruses. 2023;15(3):799.
837 doi:10.3390/v15030799

838 16. Pereira TN, Virginio F, Souza JI, Moreira LA. Emergent arboviruses: a
839 review about Mayaro virus and Oropouche orthobunyavirus. Front Trop
840 Dis. 2021;2:737436. doi:10.3389/fitd.2021.737436

841 17. de Thoisy B, Gardon J, Alba Salas R, Morvan J, Kazanji M. Mayaro virus
842 in wild mammals, French Guiana. Emerg Infect Dis. 2003;9(10):1326–
843 1329. doi:10.3201/eid0910.030161

844 18. Silva-Ramos CR, Mejorano-Fonseca JA, Hidalgo M, Rodríguez-Morales
845 AJ, Faccini-Martínez ÁA. Clinical, epidemiological, and laboratory features

of Mayaro virus infection: a systematic review. Curr Trop Med Rep. 2023;10(4):309–319. doi:10.1007/s40475-023-00308-6

19. de Curcio JS, Salem-Izacc SM, Pereira Neto LM, Nunes EB, Anunciação CE, Silveira-Lacerda EP. Detection of Mayaro virus in Aedes aegypti mosquitoes circulating in Goiânia, Brazil. Microbes Infect. 2022;24(4):104948. doi:10.1016/j.micinf.2022.104948

20. Brasil P, Pereira JP Jr, Moreira ME, Ribeiro Nogueira RM, Damasceno L, Wakimoto M, et al. Zika virus infection in pregnant women in Rio de Janeiro. N Engl J Med. 2016;375(24):2321–2334. doi:10.1056/NEJMoa1602412

21. Vermillion MS, Lei J, Shabi Y, Baxter VK, Crilly NP, McLane M, et al. Intrauterine Zika virus infection of pregnant immunocompetent mice models transplacental transmission and adverse perinatal outcomes. Nat Commun. 2017;8:14575. doi:10.1038/ncomms14575

22. Ramful D, Carbonnier M, Pasquet M, Bouhmani B, Ghazouani J, Noormahomed T, et al. Mother-to-child transmission of chikungunya virus infection. Pediatr Infect Dis J. 2007;26(9):811–815. doi:10.1097/INF.0b013e3180616d4f

23. Gérardin P, Barau G, Michault A, Bintner M, Randrianaivo H, Choker G, et al. Multidisciplinary prospective study of mother-to-child chikungunya virus infections on the island of La Réunion. PLoS Med. 2008;5(3):e60. doi:10.1371/journal.pmed.0050060

24. Pancetti FGM, Honório NA, Urbinatti PR, Lima-Camara TN. Twenty-eight years of Aedes albopictus in Brazil: a rationale to maintain active

870 entomological and epidemiological surveillance. Rev Soc Bras Med Trop.
871 2015;48(1):87–89. doi:10.1590/0037-8682-0155-2014

872 25. Mota MT, Costa VV, Sugimoto MA, Guimarães GF, Queiroz-Junior CM,
873 Moreira TP, et al. In-depth characterization of a novel live-attenuated
874 Mayaro virus vaccine candidate using an immunocompetent mouse model.
875 Sci Rep. 2020;10:5306. doi:10.1038/s41598-020-62084-x

876 26. Santos FM, Dias RS, de Oliveira MD, Costa ICTA, Fernandes LS, Pessoa
877 CR, et al. Animal model of arthritis and myositis induced by the Mayaro
878 virus. PLoS Negl Trop Dis. 2019;13(5):e0007375.
879 doi:10.1371/journal.pntd.0007375

880 27. da Silva Caetano CC, Camini FC, Almeida LT, Ferraz AC, da Silva TF,
881 Lima RLS, et al. Mayaro virus induction of oxidative stress is associated
882 with liver pathology in a non-lethal mouse model. Sci Rep. 2019;9:12347.
883 doi:10.1038/s41598-019-51713-9

884 28. de Carvalho AC, Dias CSB, Coimbra LD, Rocha RPF, Borin A, Fontoura
885 MA, et al. Characterization of systemic disease development and paw
886 inflammation in a susceptible mouse model of Mayaro virus infection. Int J
887 Mol Sci. 2023;24(5):4799. doi:10.3390/ijms24054799

888 29. Rosa RB, de Castro EF, de Oliveira Santos D, da Silva MV, Pena LJ. Mouse
889 models of Mayaro virus. Viruses. 2023;15(9):1803. doi:10.3390/v15091803

890 30. Acosta-Ampudia Y, Monsalve DM, Rodríguez Y, Pacheco Y, Anaya JM,
891 Ramírez-Santana C. Mayaro: an emerging viral threat? Emerg Microbes
892 Infect. 2018;7(1):163. doi:10.1038/s41426-018-0163-5

893 31. Weger-Lucarelli J, Carrau L, Levi LI, Rezelj V, Vallet T, Blanc H, et al.
894 Host nutritional status affects alphavirus virulence, transmission, and
895 evolution. PLoS Pathog. 2019;15(11):e1008089.
896 doi:10.1371/journal.ppat.1008089

897 32. Powers AM, Aguilar PV, Chandler LJ, Brault AC, Meakins TA, Watts D,
898 et al. Genetic relationships among Mayaro and Una viruses suggest distinct
899 patterns of transmission. Am J Trop Med Hyg. 2006;75(3):461–469.
900 doi:10.4269/ajtmh.2006.75.461

901 33. Chuong C, Bates TA, Weger-Lucarelli J. Infectious cDNA clones of two
902 strains of Mayaro virus for studies on viral pathogenesis and vaccine
903 development. Virology. 2019;535:227–231.
904 doi:10.1016/j.virol.2019.07.013.

905 34. Figueiredo CM, Neris RLS, Gavino-Leopoldino D, da Silva MOL, Almeida
906 JS, dos Santos JS, et al. Mayaro virus replication restriction and induction
907 of muscular inflammation in mice are dependent on age, type I interferon
908 response, and adaptive immunity. Front Microbiol. 2019;10:2246.
909 doi:10.3389/fmicb.2019.02246

910 35. Whitten WK. Modification of the oestrous cycle of the mouse by external
911 stimuli associated with the male. J Endocrinol. 1956;13(4):399–404.
912 doi:10.1677/joe.0.0130399

913 36. Roszkowski M, Mansuy IM. High-efficiency RNA extraction from sperm
914 cells using guanidinium thiocyanate supplemented with tris(2-
915 carboxyethyl)phosphine. Front Cell Dev Biol. 2021;9:648274.
916 doi:10.3389/fcell.2021.648274

917 37. Zhou Y, Zhou B, Pache L, Chang M, Khodabakhshi AH, Tanaseichuk O, et
918 al. Metascape provides a biologist-oriented resource for the analysis of
919 systems-level datasets. Nat Commun. 2019;10(1):1523.
920 doi:10.1038/s41467-019-09234-6

921 38. Llamas-González YY, Campos D, Pascale JM, Arbiza J, González-
922 Santamaría J. A functional ubiquitin-proteasome system is required for
923 efficient replication of New World Mayaro and Una alphaviruses. Viruses.
924 2019;11(4):370. doi:10.3390/v11040370

925 39. Valdés-Torres P, Campos D, Bhakta M, Galán-Jurado PE, Durant-
926 Archibold AA, González-Santamaría J. Honokiol and alpha-mangostin
927 inhibit Mayaro virus replication through different mechanisms. Molecules.
928 2022;27(21):7362. doi:10.3390/molecules27217362

929 40. Megli CJ, Coyne CB. Infections at the maternal–fetal interface: an overview
930 of pathogenesis and defence. Nat Rev Microbiol. 2022;20(2):67–82.
931 doi:10.1038/s41579-021-00610-y

932 41. Hcini N, Lambert V, Picone O, Carod JF, Carles G, Pomar L, et al.
933 Arboviruses and pregnancy: are the threats visible or hidden? Trop Dis
934 Travel Med Vaccines. 2024;10(1):1–12. doi:10.1186/s40794-023-00213-w

935 42. Atkins GJ, Carter J, Sheahan BJ. Effect of alphavirus infection on mouse
936 embryos. Infect Immun. 1982;35(2):546–553.

937 43. Taylor M, Rayner JO. Immune response to chikungunya virus: sex as a
938 biological variable and implications for natural delivery via the mosquito.
939 Viruses. 2023;15(9):1869. doi:10.3390/v15091869

44. Hoen B, Schaub B, Funk AL, Ardillon V, Boullard M, Cabié A, et al. Pregnancy outcomes after ZIKV infection in French territories in the Americas. N Engl J Med. 2018;378(11):985–994. doi:10.1056/NEJMoa1709481

45. Wu Y, Su K, Zhang Y, Liang L, Wang F, Chen S, et al. A spatiotemporal transcriptomic atlas of mouse placentation. Cell Discov. 2024;10(1):74. doi:10.1038/s41421-024-00740-6

46. European Parliament, Council of the European Union. Directive 2010/63/EU on the protection of animals used for scientific purposes. 2010. Available from: https://eur-lex.europa.eu/legal-content/EN/TXT/?uri=CELEX:32010L0063

47. National Research Council (US). Recognition and alleviation of pain in laboratory animals. Washington (DC): National Academies Press; 2009

48. Rosa RB, De Castro EF, De Oliveira Santos D, Dantas WM, Tanaka CA, Mendes RPG, et al. A comprehensive murine clinical model for development of countermeasures and studying Mayaro virus infection. PLoS Negl Trop Dis. 2025;19(7):e0013333. doi:10.1371/journal.pntd.0013333

ACKNOWLEDGMENTS

We thank José González Santamaría from the Department of Genomics and Proteomics Research, Gorgas Memorial Institute for Health Studies, Panama, for providing the primary antibody used in this study.

AUTHOR CONTRIBUTIONS

Conceptualization: APA, GM and MC. Methodology: APA, PP, JLP, MPG, BV, JMV, GM and MC. Investigation: APA, PP, JLP, MPG, GG, BV, JMV, GM and MC. Visualization: APA, PP, JLP, MPG, GG, BV, JMV, GM and MC. Statistical Analysis: APA. Supervision: GM and MC. Writing—original draft: APA, PP, JLP, GG, JMV, GM and MC. Writing—review & editing: APA, PP, JLP, MPG, GG, JH, AF, BV, JMV, GM and MC. Project administration: GM and MC. Funding acquisition: GM and MC. All authors agreed to submit the manuscript and have read and approved its final version. Authors take full responsibility for its content.

FUNDING

Institut Pasteur de Montevideo and FOCEM (COF 03/11), G4 program Institut Pasteur de Montevideo.

COMPETING INTERESTS

The authors declare no competing interests.